24 January 2022

Dear Associate Editor,

Dear Dr. Claire Masteller,

Please find below a detailed point-by-point response (black) to all referee comments (blue). Revised paragraphs of the manuscript are reproduced with tracked changes (new text, ~~removed text~~) below our responses. Revised figures are also provided alongside their original versions for comparison.

We hope you appreciate our response to their constructive remarks, and that you will consider this revised version for publication in *Earth Surface Dynamics*. We want to sincerely thank you and the referees for helping to improve our manuscript.

Best regards,

Olivier Gourgue

Referee #1

This paper presents a biogeomorphic model applied to a specific tidal marsh restoration project in the Scheldt Estuary. The authors demonstrate model performance by way of application, comparing modeling results with morphological and ecological features of an active salt marsh located close to the restoration site. It is demonstrated that different options in the restoration scheme can critically lead to different evolutionary trajectories of the restored marsh, both in terms of morphological and ecological developments in space and time. The innovative side of the model lies in the fact that it combines different numerical techniques to couple both fine-scale vegetation dynamics and vegetation-flow interactions (occurring at sub metric scales) and the ecomorphodynamic evolution of the overall marsh systems (at km^2 scale). I have read the paper very carefully and found it much interesting and very well written. I only have minor comments that I'd like to submit to the authors before the paper can be published.

We thank the referee for their careful review of our manuscript, as well as for their positive and constructive remarks.

Major comments

l.230: It would be interesting to compare the values of SLR rates used here with the IPCC SLR projections for the same study area, to put the values used in this study in a proper context.

IPCC sea level rise rate projections for the period 2005-2055 at the estuary mouth range between 4.8 and 6.3 mm/yr. These are median projections for Representative Concentration Pathways 2.6 and 8.5 (IPCC, 2019). This is very much consistent with the reference value of 6 mm/yr used in our study. However, we also explain in the manuscript that this value of 6 mm/yr rather corresponds to the average rate of mean high-water level rise observed in the Scheldt Estuary over the last century, likely influenced by both global sea level rise and human-induced changes in the geomorphology of the estuary, such as dredging and dike construction. These local IPCC projections also illustrate that our two additional scenarios (i.e., 0 and 12 mm/yr) are rather extreme. We can therefore reasonably assume that our study covers the range of possible future sea level rise rates in the area.

Sect. 2.3.1 (1st paragraph)

We investigate the resilience of the restored tidal marsh to human-induced climate and environmental changes by considering different relative SLR rates and different SSC at the seaward boundary (Table 1). If our model can account for changes in MSL (Sect. 2.1), changes in MHWL are more relevant for the biogeomorphology of tidal marshes, as the intertidal elevation relative to MHWL determines the tidal inundation regime, hence affecting sediment accretion rates (Temmerman et al., 2004) and vegetation growth (Balke et al., 2016). Therefore, for the reference model scenario, we consider a SLR rate corresponding to the average rate of MHWL rise observed in the Scheldt Estuary over the last century, that is, 6 mm yr^{-1} (Temmerman et al., 2004; Wang and Temmerman, 2013). This relatively high rate of MHWL rise is partly due to global

SLR but also likely amplified by local human-induced changes in the geomorphology of the estuary, such as historical embankment of intertidal areas and widening and deepening of the navigation channels (Smolders et al., 2015; Wang et al., 2019). We also consider two additional scenarios, with no (0 mm yr^{-1}) and high (12 mm yr^{-1}) SLR rate, respectively. In comparison, SLR rate projections for the period 2005-2055 at the estuary mouth range between 4.8 and 6.3 mm/yr (median projections for Representative Concentration Pathways 2.6 and 8.5 – IPCC, 2019). With these relatively extreme additional scenarios, we can therefore reasonably assume that we cover the range of possible future SLR rates in the area.

l.295: I am not entirely sure it is correct to refer to O'Brien's law here. The reason is twofold. First, the classic O'Brien's law is derived based on the tidal prism computed within tidal channels (not the overmarsh tidal prism as it was done here). Second, the exponent of the power-law relationship in O'Brien's law is well defined and typically equals ~6/7, which is quite different from the values proposed here (perhaps because of the difference in the way tidal prism is computed, as said before). Therefore, I'd rather refer to a generic tidal prism vs. cross-sectional channel area, without invoking O'Brien's law.

We agree that we should not refer to O'Brien's law in our analysis of channel cross-section surface area vs. overmarsh tidal prism. To remain consistent with the observations against which we compare our model results, we here follow the approach used by Vandenbruwaene et al. (2013, 2015) who argue that overmarsh tides (i.e., which overtop the mash platform level) are especially relevant in such analysis for tidal marsh channels, because maximum channel flow velocities typically occur when the surrounding platform is flooded and drained (Bayliss-Smith et al., 1979; Pethick, 1980; French and Stoddart, 1992). We have removed all references to O'Brien's law in the revised manuscript.

Sect. 2.4.3

Channel networks control the flow of water and sediments in tidal marshes, and their evolution interact with the biogeomorphic development of the surrounding intertidal platforms (D'Alpaos et al., 2007; Kearney and Fagherazzi, 2016). Here, we compare various geometric properties of the simulated tidal channels with observations in the adjacent marshes of the Drowned Land of Saeftinghe (Fig. 2c – Vandenbruwaene et al., 2013, 2015). To that end, we have developed a quasi-automatic methodology to extract tidal channel networks and related geometric properties from model results. More specifically, we compute the probability distribution of unchanneled flow length (i.e., the shortest distance to a channel bank) as a measure of channel density (Tucker et al., 2001). The mean unchanneled flow length is calculated as the slope of the linear portion of the probability distribution when plotted on semi-log axes (Marani et al., 2003; Chirol et al., 2018). Along the channel network skeleton (i.e., the channel centerlines – Fagherazzi et al., 1999), we compute the watershed area, the upstream mainstream channel length (i.e., the longest upstream channel within the watershed), the mean overmarsh tidal prism (i.e., the mean high-tide water volume within the watershed for all tides overtopping the surrounding platform – Vandenbruwaene et al., 2013, 2015) and the channel cross-sectional dimensions (i.e., channel width, channel depth and channel cross-section area). We also verify the applicability of Hack's

law, an empirical power relationship that links watershed area and mainstream channel length (Rigon et al., 1996). ~~We also verify the applicability of O'Brien's law, an empirical relationship that links tidal prism and channel cross-section area (D'Alpaos et al., 009, 2010).~~ See Sect. S4 (supplementary material) for more details.

Sect. 3.2 (2nd paragraph)

The predicted channel network 50 years after de-embankment is slightly less dense, as compared with observations in a nearby tidal marsh (Fig. 4a), with mean unchanneled flow lengths of respectively 26.0 m (model) and 23.7 m (observations). The exponent of Hack's law is 0.908 for the model results and 0.909 for the observations (Fig. 4b). These values are statistically equal as the slopes of the linear regressions are not significantly different ($p = 0.913$ – Table S2, supplementary material). However, their intercepts are significantly different ($p = 0.007$), which means that the predicted channel lengths are smaller than those observed in the nearby natural marsh, with regards to the local watershed area. The exponent of ~~O'Brien's law~~ the power law in Fig. 4e is 0.71 for the model results and 0.87 for the observations ~~(Fig. 4e)~~. These values are not statistically equal as the slopes of the linear regressions are slightly, but significantly different ($p = 0.023$). The intercepts are also significantly different ($p = 0.004$), which means that predicted channel cross-section areas are larger than those observed in the nearby tidal marsh, with regards to the local tidal prism. The relatively important deviations between model results and observations in terms of channel width and channel depth (Fig. 4c-d and Table S2, supplementary material) partly compensate each other, so that the discrepancy in channel cross-section area is much smaller, but also decreases with increasing tidal prism (Fig. 4e).

Sect. S4 (3rd paragraph)

Cross-sectional dimensions of tidal channels are traditionally related to the spring tidal prism (D'Alpaos et al., 2010). For tidal marsh channels, however, overmarsh tides that overtop the intertidal platform are more relevant (Vandenbruwaene et al., 2013, 2015) because maximum channel flow velocities typically occur when the surrounding platform is flooded and drained (Bayliss-Smith et al., 1979; Pethick, 1980; French and Stoddart, 1992). Here we use the mean overmarsh tidal prism, defined as the mean tidal prism from all overmarsh tides. For every point along the network skeleton, we compute the mean platform elevation of the corresponding watershed. The mean overmarsh tidal prism is then simply the product between the watershed area and the mean overmarsh high-water depth, obtained from all simulated high tides higher than the mean platform elevation.

Fig. 4 (original)

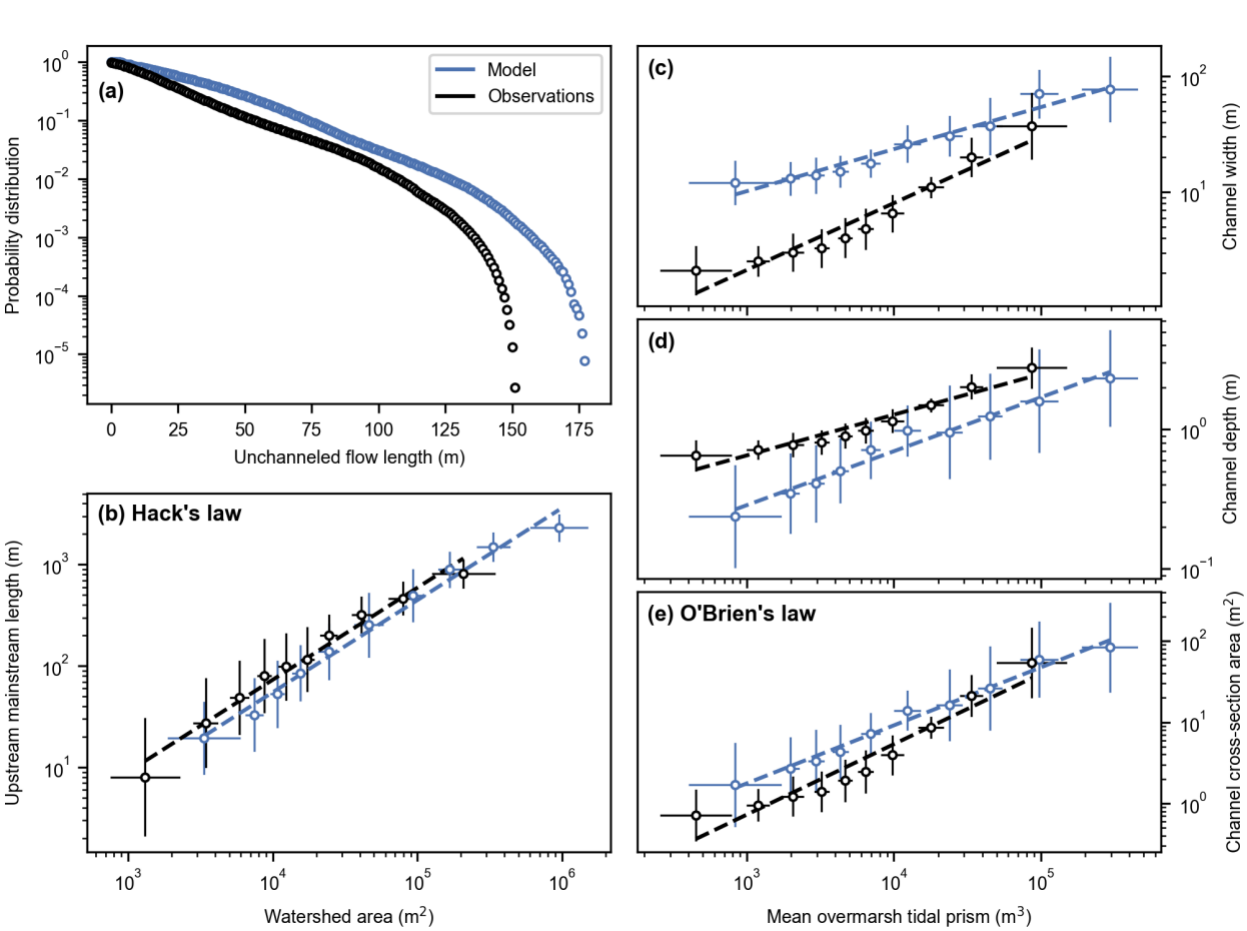

Figure 4: Reference model scenario (#1). Channel geometric properties 50 years after de-embankment (blue) compared to observations in an established marsh close to the study site (black). Probability distribution of the unchanneled flow length (a), upstream mainstream length vs. watershed area (b), and channel width (c), channel depth (d) and channel cross-section area (e) vs. mean overmarsh tidal prism. (b-e) Model results and observations are respectively split into 10 sub-samples of equal size (Sect. 2.4.4). Markers and error bars represent the geometric means and standard deviations of each sub-sample, respectively. Dashed lines represent geometric regressions of the geometric means.

Fig. 4 (revised)

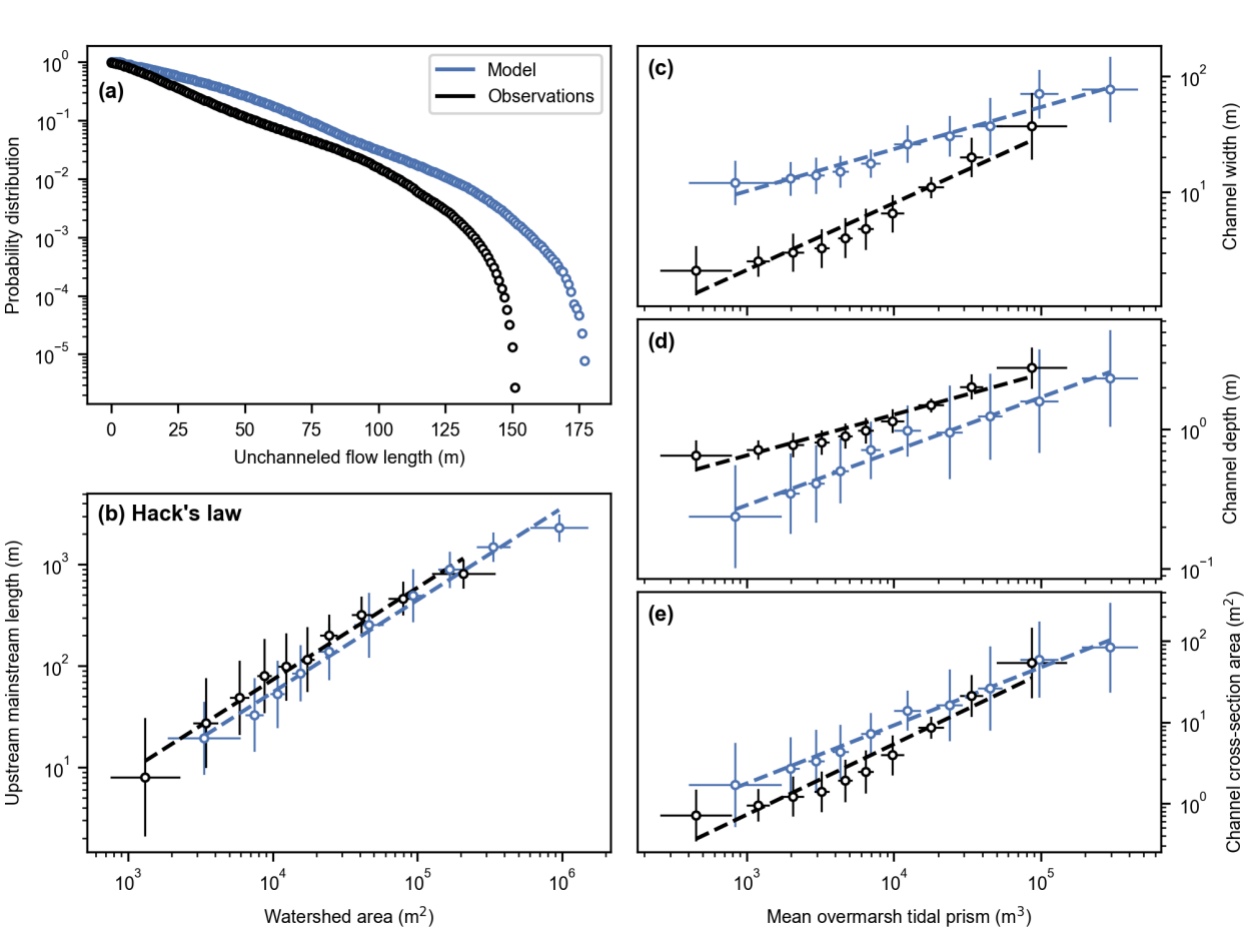

Figure 4: Reference model scenario (#1). Channel geometric properties 50 years after de-embankment (blue) compared to observations in an established marsh close to the study site (black). Probability distribution of the unchanneled flow length (a), upstream mainstream length vs. watershed area (b), and channel width (c), channel depth (d) and channel cross-section area (e) vs. mean overmarsh tidal prism. (b-e) Model results and observations are respectively split into 10 sub-samples of equal size (Sect. 2.4.4). Markers and error bars represent the geometric means and standard deviations of each sub-sample, respectively. Dashed lines represent geometric regressions of the geometric means.

Fig. S7 (original)

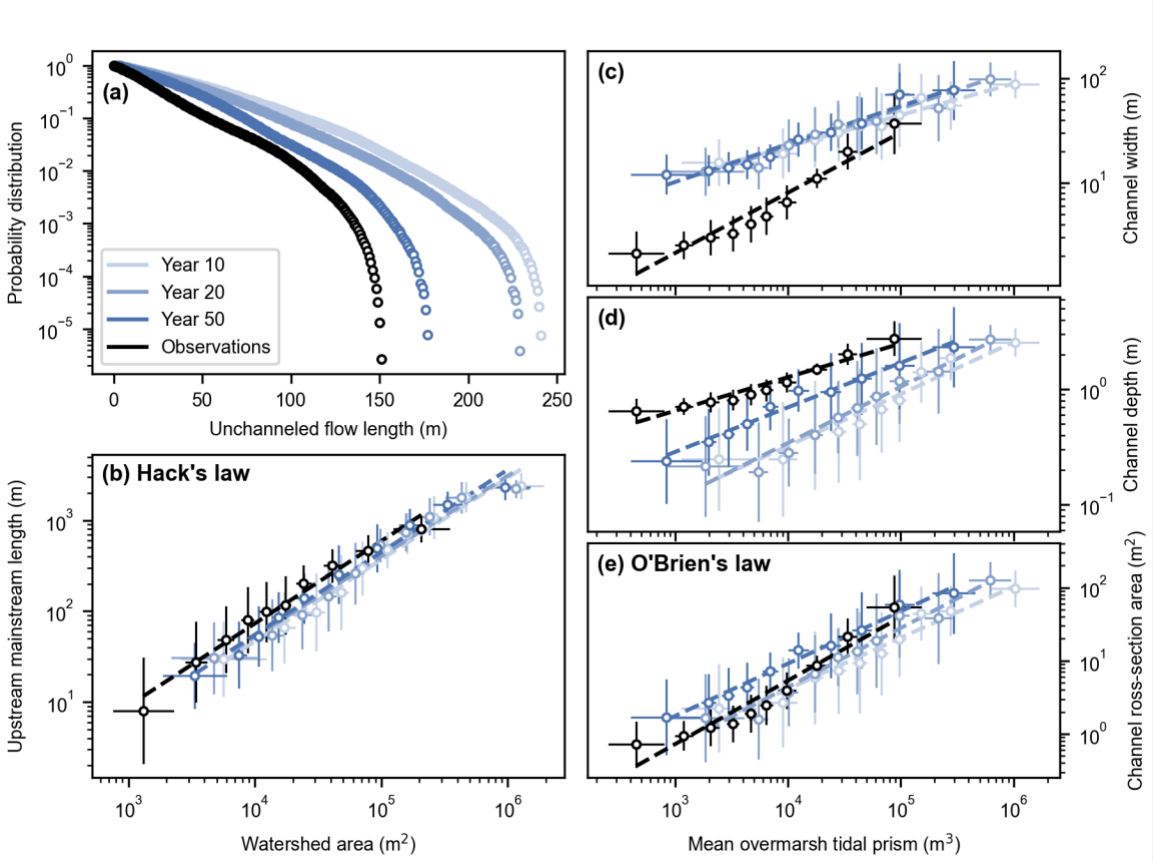

Figure S7: Reference model scenario (#1). Channel geometric properties 10, 20 and 50 years after de-embankment (different shades of blue) compared to observations in an established marsh nearby the study site (black). Probability distribution of the unchanneled flow length (a), upstream mainstream length vs. watershed area (b), and channel width (c), channel depth (d) and channel cross-section area (e) vs. mean overmarsh tidal prism. (b-e) Model results and observations are respectively split into 10 sub-samples of equal size (Sect. 2.4.4). Markers and error bars represent the geometric means and standard deviations of each sub-sample. Dashed lines represent geometric regressions of the geometric means.

Fig. S7 (revised)

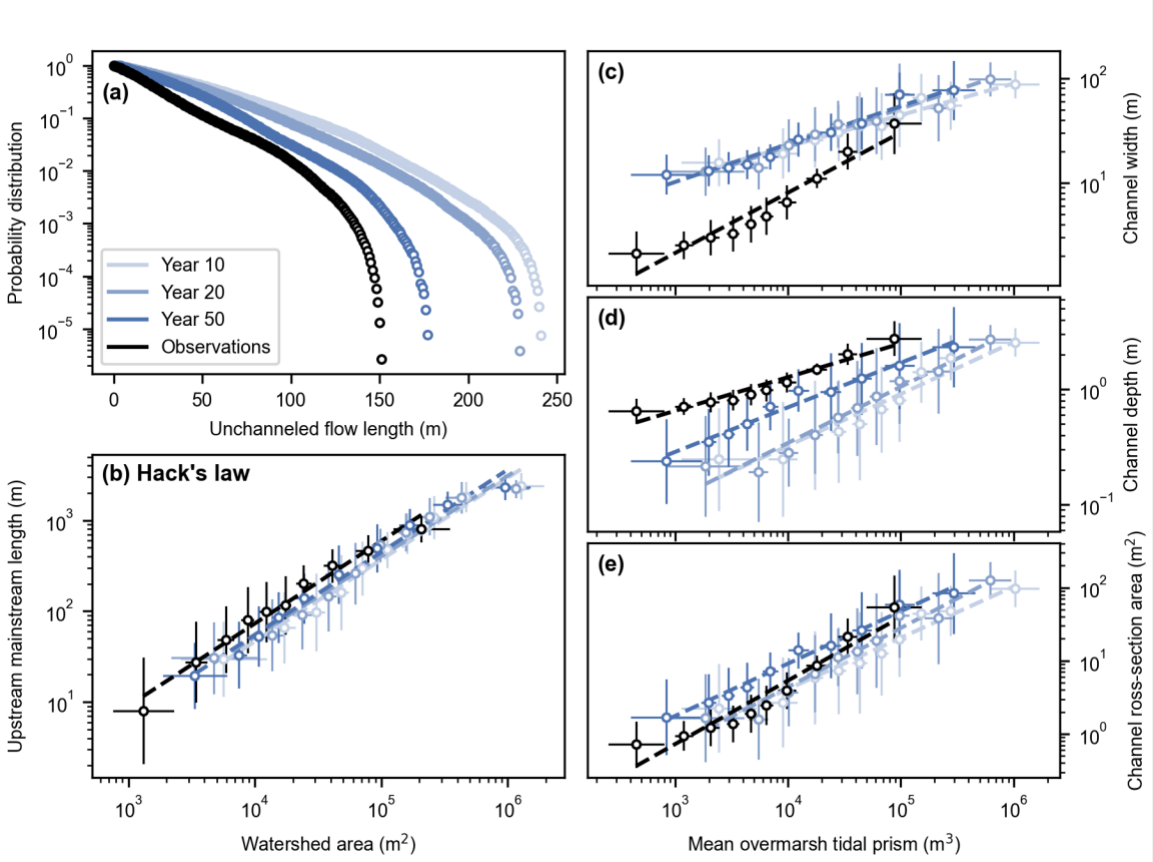

Figure S7: Reference model scenario (#1). Channel geometric properties 10, 20 and 50 years after de-embankment (different shades of blue) compared to observations in an established marsh nearby the study site (black). Probability distribution of the unchanneled flow length (a), upstream mainstream length vs. watershed area (b), and channel width (c), channel depth (d) and channel cross-section area (e) vs. mean overmarsh tidal prism. (b-e) Model results and observations are respectively split into 10 sub-samples of equal size (Sect. 2.4.4). Markers and error bars represent the geometric means and standard deviations of each sub-sample. Dashed lines represent geometric regressions of the geometric means.

Fig. S8 (original)

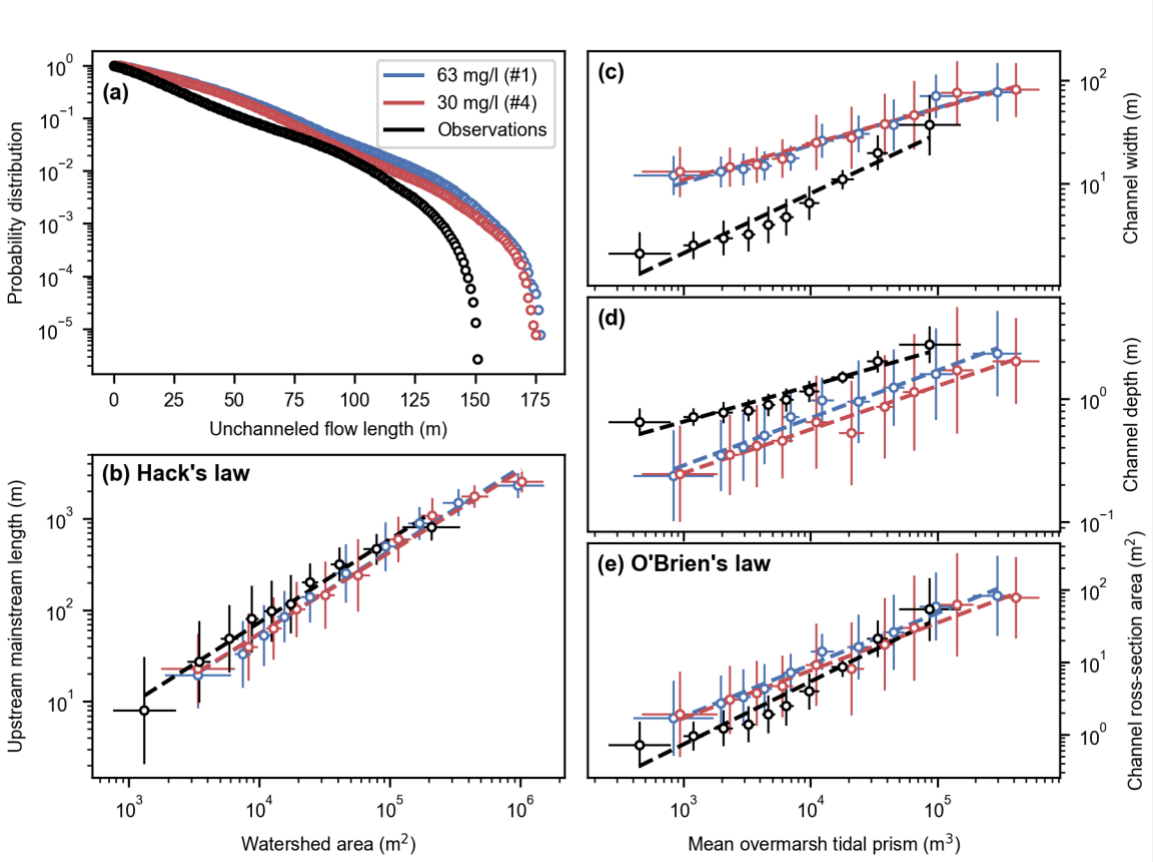

Figure S8: Suspended sediment concentration model scenarios (#1, 4). Channel geometric properties 50 years after de-embankment (blue, red) compared to observations in an established marsh nearby the study site (black). Probability distribution of the unchanneled flow length (a), upstream mainstream length vs. watershed area (b), and channel width (c), channel depth (d) and channel cross-section area (e) vs. mean overmarsh tidal prism. (b-e) Model results and observations are respectively split into 10 sub-samples of equal size (Sect. 2.4.4). Markers and error bars represent the geometric means and standard deviations of each sub-sample. Dashed lines represent geometric regressions of the geometric means.

Fig. S8 (revised)

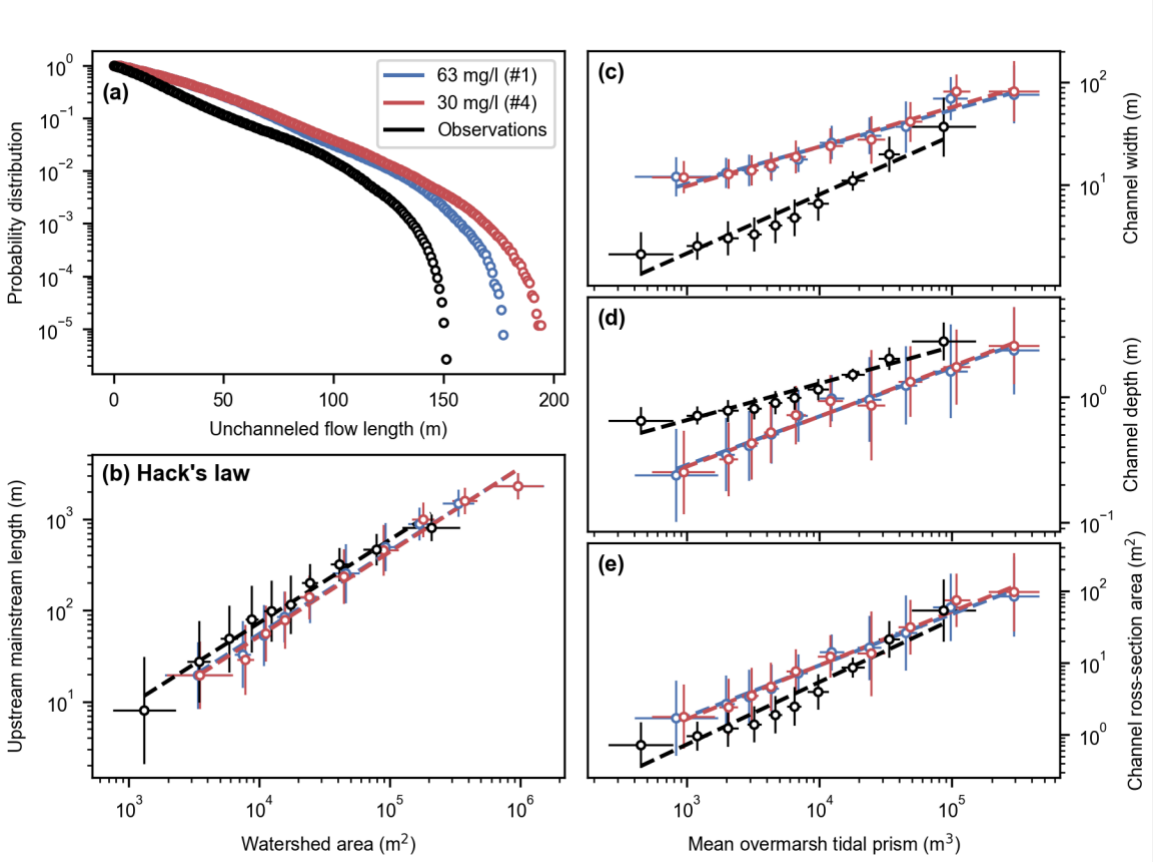

Figure S8: Suspended sediment concentration model scenarios (#1, 4). Channel geometric properties 50 years after de-embankment (blue, red) compared to observations in an established marsh nearby the study site (black). Probability distribution of the unchanneled flow length (a), upstream mainstream length vs. watershed area (b), and channel width (c), channel depth (d) and channel cross-section area (e) vs. mean overmarsh tidal prism. (b-e) Model results and observations are respectively split into 10 sub-samples of equal size (Sect. 2.4.4). Markers and error bars represent the geometric means and standard deviations of each sub-sample. Dashed lines represent geometric regressions of the geometric means.

l.365: This is perhaps too big of a step since the propagation of suspended sediment depends not only on the tidal prism but also on well-known processes of sediment advection and dispersion. In fact, sediment transport of suspended sediment is by no means related to the tidal prism, the latter being only related to the channel cross-section as clearly demonstrated by the cited O'Brien's law, according to which the size (i.e., cross-section) of the channel depends on the flowing tidal prism regardless of the concentration sediments carried in suspension by tidal flows. This applies also to l.544-545.

We agree and have removed these sentences from the revised manuscript.

Sect. 3.2 (2nd paragraph)

The predicted channel network 50 years after de-embankment is slightly less dense, as compared with observations in a nearby tidal marsh (Fig. 4a), with mean unchanneled flow lengths of respectively 26.0 m (model) and 23.7 m (observations). The exponent of Hack's law is 0.908 for the model results and 0.909 for the observations (Fig. 4b). These values are statistically equal as the slopes of the linear regressions are not significantly different ($p = 0.913$ – Table S2, supplementary material). However, their intercepts are significantly different ($p = 0.007$), which means that the predicted channel lengths are smaller than those observed in the nearby natural marsh, with regards to the local watershed area. The exponent of the power law in Fig. 4e is 0.71 for the model results and 0.87 for the observations. These values are not statistically equal as the slopes of the linear regressions are slightly, but significantly different ($p = 0.023$). The intercepts are also significantly different ($p = 0.004$), which means that predicted channel cross-section areas are larger than those observed in the nearby tidal marsh, with regards to the local tidal prism. The relatively important deviations between model results and observations in terms of channel width and channel depth (Fig. 4c-d and Table S2, supplementary material) partly compensate each other, so that the discrepancy in channel cross-section area is much smaller, but also decreases with increasing tidal prism (Fig. 4e). ~~This suggests that appropriate volume of water, and hence suspended sediments, are conveyed through the channel network and towards the intertidal platforms.~~

Sect. 4.2 (3rd paragraph)

Studies that evaluate the performance of a tidal marsh biogeomorphic model against field observations of marsh development over relevant spatio-temporal scales (several km² and decades) are rather scarce. In this paper, we show that our model results are in relatively good agreement with observations from tidal marshes close to the study site, in terms of sediment accretion rates on vegetated platforms (Fig. S4, supplementary material), vegetation cover development (Fig. S5, supplementary material) and channel geometric properties (Fig. 4). The discrepancies between model results and observations in channel width and channel depth, and to a lesser degree in channel cross-section area, may be related to different factors. With a spatial resolution of 5 m, the model is unable to develop channels narrower than 10 to 20 m, while the observations come from remote sensing images with a spatial resolution of 50 cm, revealing channel widths as narrow as a few meters (Fig. 4c). Concomitantly, if the model overestimates the width of channels, this leads to a lower capacity for flow concentration and channel deepening through erosion, which can explain why the model predicts shallower channels, as compared to observations (Fig. 4d). Moreover, observations come from a much older marsh, which was also created by dike breaching of a former polder area, but around 400 years ago (Jongepier et al., 2015). Fifty years after de-embankment, our restored tidal marsh is probably still at an earlier stage of development, as compared to the reference marsh. D'Alpaos et al. (2006) show that the width-to-depth ratio of channels decreases with marsh age. This is line with our model results, which indicate that channel depth increases over time, although channel width remains stable (Fig. S7, supplementary material), probably because of the grid resolution limitations discussed above. Finally, the SSC in the estuary is on average 1.5 times higher in the vicinity of the study site, as compared to the adjacent reference marsh where observations come from (Sect. S2, supplementary material). However, our model results indicate that even reducing

the sediment availability by a factor of 2 has nearly no impact on the channel geometric properties (Fig. S8, supplementary material). In any case, discrepancies in channel cross-section area are much smaller, as compared to channel width and channel depth, and they decrease with tidal prism (Fig. 4e). ~~This suggests that appropriate volume of water, and hence suspended sediments, are conveyed through the channel network and towards the intertidal platforms.~~

I'd be curious to know model sensitivity to some of the input parameters, in particular those related to vegetation lateral expansion (e.g., R_i^{exp}). I think these parameters are critical in determining the evolution of marsh vegetation through time.

We have explored the model sensitivity to various vegetation input parameters, including the lateral expansion rate R_i^{exp}, but not in a systematic way for the present study. This is a very relevant topic, but we have already addressed it in a previous paper (Schwarz et al., 2018) and we further explore it in another paper in preparation. In general, fast colonizers (characterized by high number of establishing seedlings that produce homogeneous vegetation patterns) favor stabilization of pre-existing channels and consolidation of the landscape configuration, while slow colonizers (characterized by low number of establishing seedlings able to expand laterally, resulting in patchy vegetation patterns) facilitate the formation of new channels and thereby actively facilitates further landscape self-organization (Schwarz et al., 2018).

However, the scope of the present paper is on tidal marsh restoration and how different restoration design options can impact the biogeomorphic development of tidal marshes. That is why our model scenarios focus on real-life restoration design options (i.e., the size of the created tidal inlets), using fixed vegetation parameter values that are representative for the species present in the area, and that are well constrained for the Scheldt Estuary based on previous field studies (e.g., Silinski et al., 2016). Adding model scenarios with various vegetation parameter values would be an interesting theoretical model experiment, but not relevant for real-life marsh restoration, and hence would deviate from the scope of this paper. Nevertheless, for the sake of completeness, we have incorporated some examples as supplementary material of the revised manuscript, which illustrate that vegetation input parameters have rather limited impact on the long-term morphodynamics in the case studied here.

Sect. 2.3.3

In the reference model scenario, vegetation establishes randomly following different colonization strategies (i.e., either homogeneously with relatively high probability of establishment but no possibility to expand laterally, or patchily with relatively low probability of establishment but possibility to expand laterally to form growing patches – Sect. S1.2, supplementary material) in areas where environmental stressors allow for it (Sect. 2.1.2). This is the expected behavior supported by field observations for the three selected species representative for pioneer, middle and high marsh vegetation (Sect. S1.5.2, supplementary material). To illustrate the impact of the vegetation dynamics on the biogeomorphic feedbacks and the model results, we also consider ~~two~~ six variants of the reference model scenario (Table

S1). ~~In the first variant, there is no vegetation. In the second variant, all species instantaneously colonize the entire areas for which environmental conditions are suitable.~~

Table S1 (new)

Table S1: Specifics of the reference model scenario variants used in Fig. S1 to S3.

Variant name	Vegetation module parameterizations
No vegetation	No vegetation module.
Instantaneous colonization	Table S5.
Low establishment probability	Table S4, but P_2^{est}, P_3^{est} and $P_{2,3}^{suc}$ divided by 10.
High establishment probability	Table S4, but P_2^{est}, P_3^{est} and $P_{2,3}^{suc}$ multiplied by 10.
Low lateral expansion rate	Table S4, but R_2^{exp}, $R_3^{exp} = 1$ m/yr.
High lateral expansion rate	Table S4, but R_2^{exp}, $R_3^{exp} = 5$ m/yr.

Sect. 3.1 (3rd paragraph)

Overall, the presence of vegetation has a positive impact on platform accretion rates in the Northern basin, although the speed of colonization has nearly no influence on the mean platform elevation 50 years after de-embankment (Fig. S1a, supplementary material). In the Southern basin, neither the presence of vegetation nor the speed of colonization seems to affect sediment accretion on the platforms (Fig. S1b, supplementary material), which suggests that the hydrodynamics is predominant in that part of the restored marsh. Locally, the vegetation dynamics can have remarkable geomorphic effects, such as the maintenance or disappearance of pre-excavated channels, whether we consider no vegetation, the reference vegetation dynamics, or instantaneous colonization (Fig. S2). In general, vegetation input parameters have a rather limited impact on the long-term morphodynamics (Fig. S3).

Fig. S3 (new)

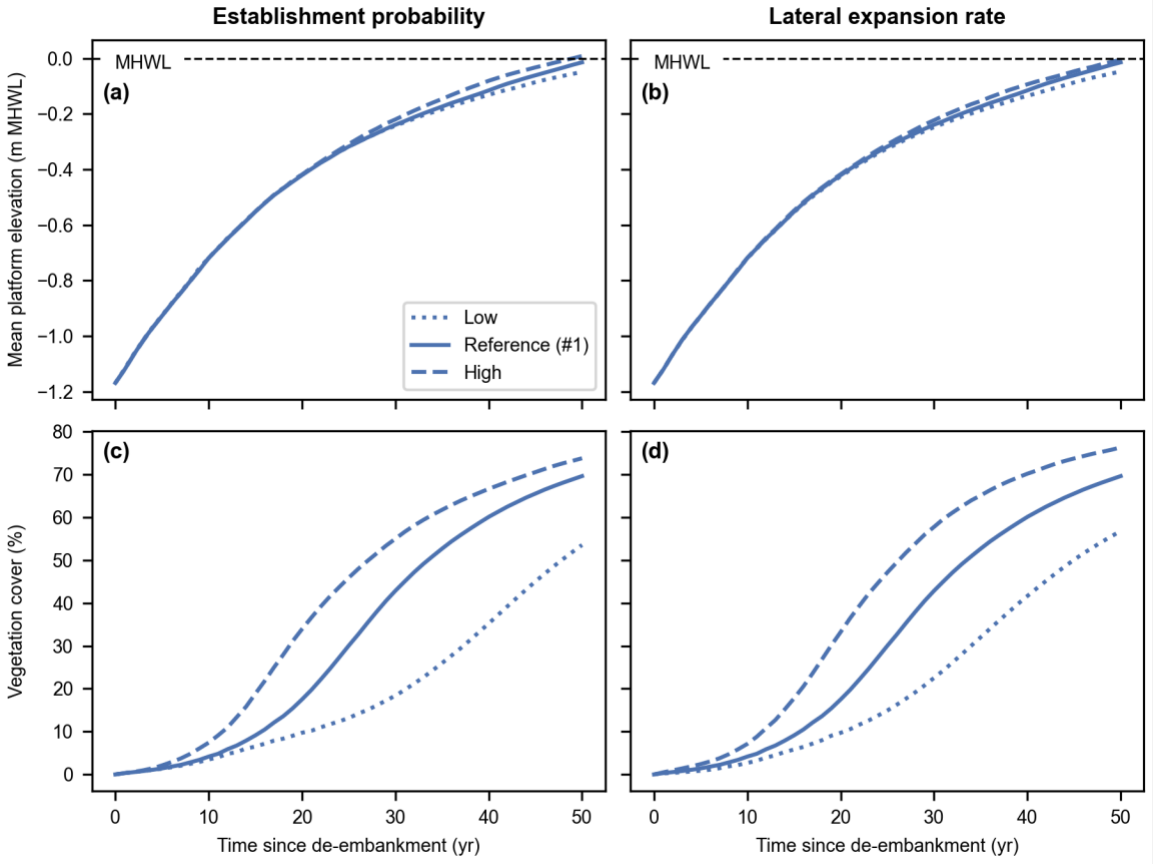

Figure S3: Vegetation input parameter model scenarios (i.e., reference vegetation dynamics and four variants, respectively with low and high establishment probability (a, c), and with low and high lateral expansion rate (b, d) – Table S1). Evolution of the mean platform elevation with respect to the mean high-water level (MHWL) (a-b) and development of the vegetation cover (c-d).

Also, the authors state that different species have different R_i^{exp}, but looking at Table S4 it seems that R_i^{exp} is held constant for all marsh perennials considered in this study. This would signify, if my interpretation is correct, that middle- and high-marsh species have nearly the same competitive ability, which I doubt is the case in real marshes.

The vegetation module is implemented such as each species can have a different mean expansion rate. In this study, the mean expansion rates for middle-marsh (*Scirpus maritimus*) and high-marsh (*Phragmites australis*) vegetation are determined based on remote sensing and literature data (see Table S3). This is pure coincidence if both species end up with the same value. However, that does not mean that both species have the same competitive ability, as the vegetation module simulates competitive interactions with a hierarchical model, where higher-rank species are stronger competitors able to outcompete lower-rank species (see Sect. S1.2 and Table S4). In our model, higher-rank species can displace lower-rank species, but not the other way around. Lower-rank species can only colonize after higher-rank species have died off. On the long term,

high-marsh vegetation (rank 3) will therefore always outcompete middle-marsh vegetation (rank 2) in its own niche.

Sect. S1.2 (new 2nd paragraph)

Our cellular automaton is implemented as a hierarchical model, where higher-rank species are stronger competitors able to outcompete lower-rank species. In our model, higher-rank species can displace lower-rank species, but not the other way around. Lower-rank species can only colonize after higher-rank species have died off. On the long term, high-rank species will therefore always outcompete lower-rank species in their own niche.

Also, related to this point, I wonder if the grid resolution for vegetation dynamics can be somehow dependent on the imposed R_i^{exp} and numerical timestep (i.e., should the resolution not exceed a certain threshold for a given R_i^{exp} and timestep to obtain reliable results with respect to vegetation dynamics)?

The grid resolution for vegetation dynamics is indeed dependent on the imposed expansion rate and numerical timestep. The number of iterations in the vegetation module (i.e., the ratio between the simulated period – one year – and the numerical time step) is determined as a function of the grid resolution and the mean expansion rate, by means of Eq. (S16) to (S19) (supplementary material).

Minor comments

l.15: add “restored” before “tidal marshes”

l.17: too generic. Explain why difficult to assess these key questions.

l.18: strange sentence…it looks like you’re applying model by dike breaching.

l.19: add a comma after “transport”

l.24: it affects -> they affect (referred to options)

l.26: to more -> higher

l.26: diversity in terms of what? Morphological? Ecological?

Abstract

There is an increasing demand for creation and restoration of tidal marshes around the world, as they provide highly valued ecosystem services. Yet, restored tidal marshes are strongly vulnerable to factors such as sea level rise and declining sediment supply. How fast the restored ecosystem develops, how resilient it is to sea level rise, and how this can be steered by restoration design, are key questions that are typically challenging to assess due to complex biogeomorphic feedback processes involved. In this paper, we apply a biogeomorphic model to

a ~~planned~~ specific tidal marsh restoration project planned by dike breaching. Our modeling approach integrates tidal hydrodynamics, sediment transport, and vegetation dynamics, accounting for relevant fine-scale flow-vegetation interactions (less than 1 m^2) and their impact on vegetation and landform development at the landscape scale (several km^2) and on the long term (several decades). Our model performance is positively evaluated against observations of vegetation and geomorphic development in adjacent tidal marshes. Model scenarios demonstrate that the restored tidal marsh can keep pace with realistic rates of sea level rise and that its resilience is more sensitive to the availability of suspended sediments than to the rate of sea level rise. We further demonstrate that restoration design options can steer marsh resilience, as ~~it affects~~ they affect the rates and spatial patterns of biogeomorphic development. By varying the width of two dike breaches, which serve as tidal inlets to the restored marsh, we show that a larger difference in the width of the two inlets leads to ~~more~~ higher biogeomorphic diversity in restored habitats. This study showcases that biogeomorphic modeling can support management choices in restoration design to optimize tidal marsh development towards sustainable restoration goals.

l.39: dams -> damming (?)

l.42: often as –> the

Sect. 1 (1st paragraph)

Tidal marshes are among the most productive ecosystems on Earth (Barbier et al., 2011) providing invaluable services such as protection of coastal settlements against storms (Gedan et al., 2011; Zhu et al. 2020), carbon sequestration (Rogers et al., 2019), maintenance of fisheries (Boesch and Turner, 1984) and water purification (Breaux et al., 1995). They are however among the most threatened ecosystems globally (Barbier et al., 2011). Over centuries, humans have built dikes to prevent tidal flooding and drained soils to gain land for agricultural, industrial, and urban expansion (Gedan et al., 2009). While human-induced degradation and loss have accelerated in recent decades (Deegan et al., 2012; Wang et al., 2014; Tian et al., 2016), remaining tidal marshes are facing the additional global threat of accelerated sea level rise (SLR) caused by climate change (Spencer et al., 2016; Schuerch et al., 2018). In addition, the capacity of tidal marshes to adapt to SLR by sediment accretion and surface elevation gain can be compromised by decreasing sediment supply, for example due to upstream river ~~dams~~ damming and erosion control measures (Weston, 2014; Yang et al., 2020). Hence, efforts for conservation and restoration of tidal marshes are increasing throughout the world (Mossman et al., 2012; Liu et al., 2016; Zhao et al., 2016; Waltham et al., 2021) with ~~often as~~ usually the primary goal to support and rehabilitate biodiversity (Armitage et al., 2007; Weinstein, 2007) and provide nursery habitat for commercially important fish and invertebrate species (Rozas and Minello, 2001). Furthermore, marsh restoration is increasingly motivated by its role for nature-based shoreline protection, as marshes attenuate waves, currents and erosion and promote sediment accretion with SLR (Kirwan and Megonigal, 2013; Temmerman et al., 2013; Barbier, 2014; Kirwan et al., 2016; Zhu et al., 2020) and for nature-based mitigation of climate change impacts through carbon sequestration (Barbier et al., 2011; Rogers et al., 2019). The success of restoration designs largely

depends on the resulting rates of marsh vegetation development and sediment accretion, as they control the timescales at which target habitats, effective shoreline protection and carbon sequestration are reached. Besides, restoration designs must enable the development of marsh ecosystems that are resilient to modern threats such as SLR and decreasing sediment supply. Yet, predicting actual rates of vegetation development and sediment accretion in establishing marshes, at timescales ranging from years to decades, remains to this day an important challenge (Fagherazzi et al., 2012; Mossman et al., 2012; Wiberg et al., 2020; Fagherazzi et al., 2020; Törnqvist et al., 2021).

l.53: landwards -> landward

l.63: add a comma after ref to Staver

Sect. 1 (2nd paragraph)

Managed realignment, which consists in shifting the line of coastal defense structures landward~~s~~ of their existing position, can create space for tidal marsh restoration or creation. This practice has grown in popularity over the last two decades (French, 2006; Turner et al., 2007), especially in the context of coastal squeeze and landward movement of the mean low water mark due to SLR and storms (Doody, 2013). Practically, a second line of defense is built landwards, while the first one is breached. The number and size of breaches are important design choices (Hood, 2014, 2015) and vary greatly between projects (e.g., Friess et al., 2014; Dale et al., 2017). As breaches become the inlets of the restored marshes, they have an important control on water and sediment volumes entering and leaving the system during each tidal cycle, and hence on sediment accretion rates (Oosterlee et al., 2020). Other important design measures may involve excavating an initial channel network and treating soil conditions to facilitate soil drainage (O'Brien and Zedler, 2006), planting manually vegetation tussocks to ensure vegetation encroachment (Staver et al., 2020), or building hydraulic structures to control the tidal range and create optimal ecological conditions for vegetation development (Maris et al., 2007; Oosterlee et al., 2018). These design choices are mainly driven by restoration objectives and local environmental conditions. Yet, there is high uncertainty in how restored tidal marshes develop. For example, several studies point at many restored sites that, in comparison with natural tidal marshes, underperform in terms of biodiversity (Wolters et al., 2005; Mossman et al., 2012), topographic diversity (Lawrence et al., 2018), groundwater dynamics (Tempest et al., 2015; Van Putte et al., 2020) and biogeochemical functioning, including carbon sequestration (Santín et al., 2009; Suir et al., 2019). These outcomes can potentially hamper marsh ecosystem functions and the initial restoration objectives.

l.110: misplaced apex in km2

Sect. 1 (6th paragraph)

In this paper, we present a biogeomorphic model application to a specific tidal marsh restoration project by managed realignment, accounting for relevant fine-scale flow-vegetation interactions (less than 1 m^2) and their impact on vegetation and landform developments at the landscape

scale (several km^2). The novelty of this paper is threefold. First, we evaluate the long-term resilience (several decades) of a large-scale restored tidal marsh project (several ~~km2~~ km^2) in response to different rates of SLR and different concentrations of suspended sediment supply. Second, we investigate how that resilience can be affected by restoration design options (here, the inlet configuration). Third, we evaluate our model performance against data on vegetation and geomorphic development in adjacent tidal marshes.

l.225: is determining -> determines

Sect. 2.3.1 (1st paragraph)

We investigate the resilience of the restored tidal marsh to human-induced climate and environmental changes by considering different relative SLR rates and different SSC at the seaward boundary (Table 1). If our model can account for changes in MSL (Sect. 2.1), changes in MHWL are more relevant for the biogeomorphology of tidal marshes, as the intertidal elevation relative to MHWL ~~is determining~~ determines the tidal inundation regime, hence affecting sediment accretion rates (Temmerman et al., 2004) and vegetation growth (Balke et al., 2016). Therefore, for the reference model scenario, we consider a SLR rate corresponding to the average rate of MHWL rise observed in the Scheldt Estuary over the last century, that is, 6 mm yr^{-1} (Temmerman et al., 2004; Wang and Temmerman, 2013). This relatively high rate of MHWL rise is partly due to global SLR but also likely amplified by local human-induced changes in the geomorphology of the estuary, such as historical embankment of intertidal areas and widening and deepening of the navigation channels (Smolders et al., 2015; Wang et al., 2019). We also consider two additional scenarios, with no (0 mm yr^{-1}) and high (12 mm yr^{-1}) SLR rate, respectively. In comparison, SLR rate projections for the period 2005-2055 at the estuary mouth range between 4.8 and 6.3 mm/yr (median projections for Representative Concentration Pathways 2.6 and 8.5 – IPCC, 2019). With these relatively extreme additional scenarios, we can therefore reasonably assume that we cover the range of possible future SLR rates in the area.

l.339: vegetated -> vegetation

Sect. 3.1 (3rd paragraph)

Overall, the presence of vegetation has a positive impact on platform accretion rates in the Northern basin, although the speed of colonization has nearly no influence on the mean platform elevation 50 years after de-embankment (Fig. S1a, supplementary material). In the Southern basin, neither the presence of vegetation nor the speed of colonization seems to affect sediment accretion on the platforms (Fig. S1b, supplementary material), which suggests that the hydrodynamics is predominant in that part of the restored marsh. Locally, the ~~vegetated~~ vegetation dynamics can have remarkable geomorphic effects, such as the maintenance or disappearance of pre-excavated channels, whether we consider no vegetation, the reference vegetation dynamics, or instantaneous colonization (Fig. S2). In general, vegetation input parameters have a rather limited impact on the long-term morphodynamics (Fig. S3).

Fig. 9: Colors are hard to differentiate in b/w printed copy.

We use the deep color palette of the Python package Seaborn throughout the paper, with each of the eight main model scenarios (Table 1) corresponding to one specific color of the nine available in that palette. We believe that this consistent use of scenario/color combination is an added value for most readers who will consult the manuscript in color. However, we agree that colors may be hard to differentiate in this specific figure for the few readers who will consult it in black and white. As the main message of this figure is that mean platform elevation and vegetation cover increase with increasing small-inlet width in the Northern basin (Fig. 9a, c) and decrease with increasing small-inlet width in the Southern basin (Fig. 9b, d), we have added arrows to highlight those trends on the figure.

Fig. 9 (original)

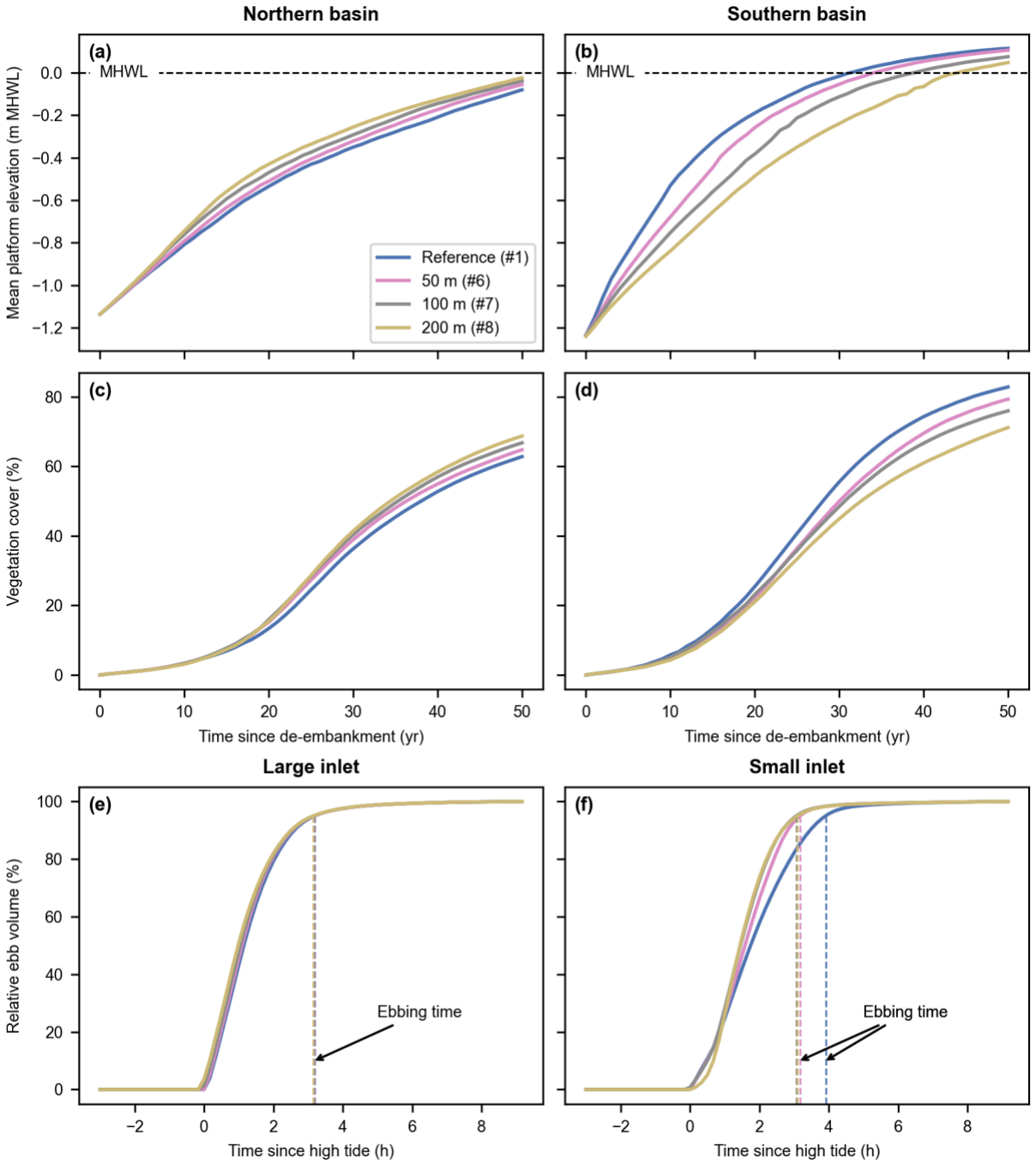

Figure 9: Inlet design model scenarios (i.e., reference design and three alternative designs with small-inlet widths of respectively 50, 100 and 200 m, and an excavated channel – #1, 6-8). Evolution of the mean platform elevation with respect to the mean high-water level (MHWL) (a-b) and development of the vegetation cover (c-d) in the Northern (a, c) and Southern basins (b, d). Evolution of the relative ebb volume (i.e., the percentage of water volume flowing through an inlet since high tide during the ebb phase, see Sect. 2.5) and resulting ebbing time (i.e., the time corresponding to a relative ebb volume of 95%, proxy for inlet flush efficiency, see Sect. 2.5) for the large (e) and small (f) inlets during a spring tide of the first year after de-embankment.

Fig. 9 (revised)

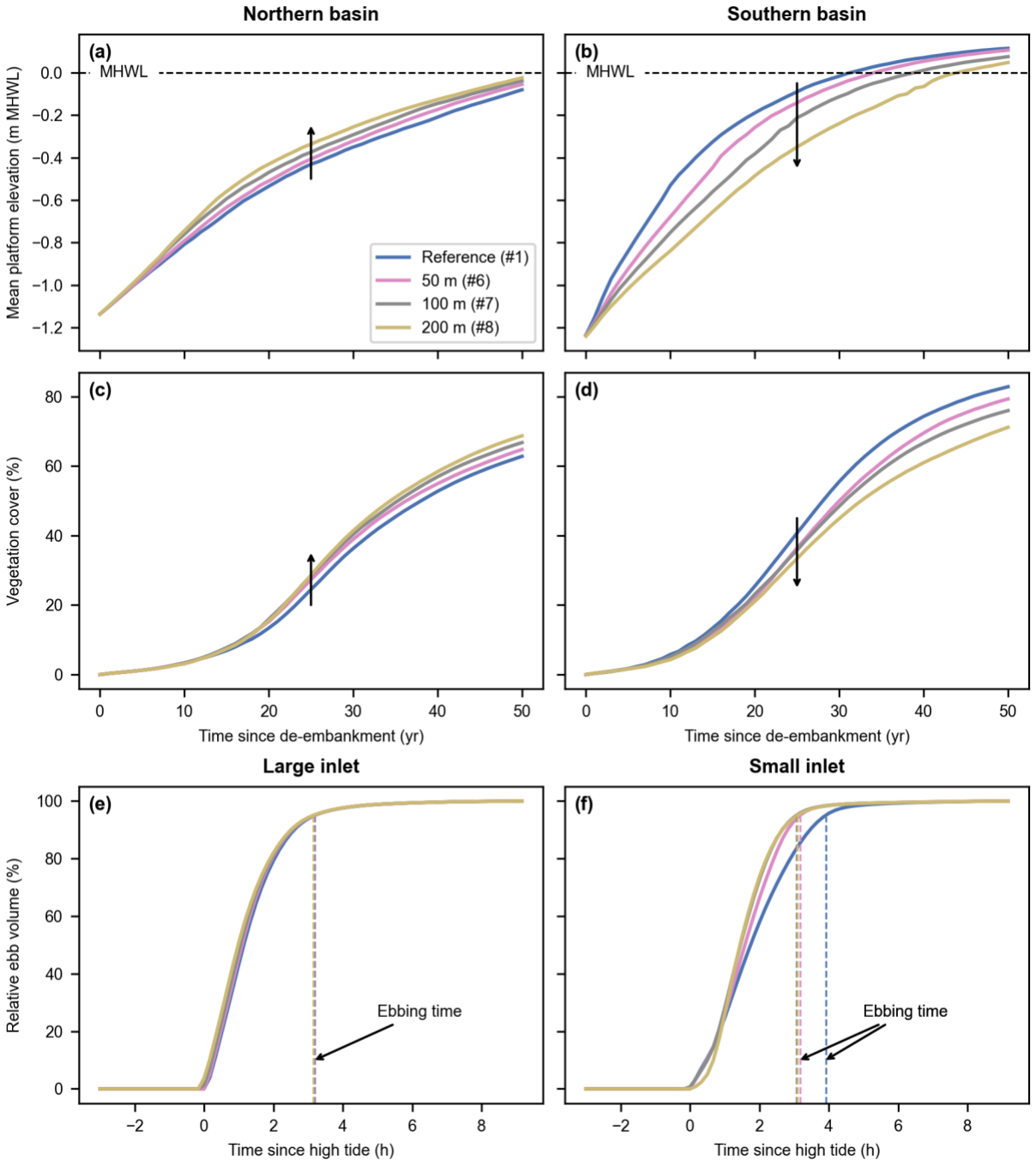

Figure 1: Inlet design model scenarios (i.e., reference design and three alternative designs with small-inlet widths of respectively 50, 100 and 200 m, and an excavated channel – #1, 6-8). Evolution of the mean platform elevation with respect to the mean high-water level (MHWL) (a-b) and development of the vegetation cover (c-d) in the Northern (a, c) and Southern basins (b, d). Evolution of the relative ebb volume (i.e., the percentage of water volume flowing through an inlet since high tide during the ebb phase, see Sect. 2.5) and resulting ebbing time (i.e., the time corresponding to a relative ebb volume of 95%, proxy for inlet flush efficiency, see Sect. 2.5) for the large (e) and small (f) inlets during a spring tide of the first year after de-embankment. Black arrows highlight trends for increasing small-inlet widths (a-d) or indicate the ebbing time (e-f).

l.473: above all -> mostly

Sect. 4.1 (1st paragraph)

One of the main objectives in every tidal marsh restoration project is for intertidal platforms to build vertically faster than SLR, allowing to develop and maintain a vegetation cover. In that context, local environmental conditions play a crucial role. In the case studied here, our model predicts that, for the first 50 years, the restored tidal marsh can keep pace with realistic rates of SLR, and that its resilience is more sensitive to suspended sediment availability (Fig. 5). These findings are in line with previous studies on marsh adaptability to SLR. For example, an ensemble model study indicates that tidal marshes with similar sediment input and tidal range as our study site can cope with SLR rates up to 70 mm yr^{-1} in the 21st century (Kirwan et al., 2010, 2016). Here, we test SLR rates up to 12 mm yr^{-1} in the first 50 years after de-embankment, for which we predict a highly resilient restored marsh. Furthermore, a recent global assessment of tidal marsh and mangrove restoration projects reveals that the ability of coastal wetlands to keep pace with SLR is ~~above all~~ mostly driven by suspended sediment availability (Liu et al., 2021), which is also in line with our results.

l.477: are depending -> depend

l.485: certain -> specific

Sect. 4.1 (2nd paragraph)

A second key question that is typically raised when planning for tidal marsh restoration is how fast the ecosystem and its different habitat zones develop (Yando et al., 2019), which is for a large part driven by the rates of sediment accretion, pioneer vegetation establishment and succession. Here, the desired rates ~~are depending~~ depend on the restoration objectives. High rates of sediment accretion and vegetation development allow to quickly reach certain restoration objectives, such as different aspects of nature-based shoreline protection. For example, high-lying and densely vegetated marshes are most effective for wave attenuation (Möller, 2006; Schoutens et al., 2020; Willemsen et al., 2020), and reduction of shoreline erosion (Möller et al., 2014; Francalanci et al., 2013; Wang et al., 2017; Schoutens et al., 2019) and dike breaching hazards (Zhu et al., 2020). However, when tidal marshes are created along estuaries or deltas to attenuate extreme high tides and storm surges (Smolders et al., 2015; Stark et al., 2017; Huguet et al., 2018; Smolders et al., 2020), lower accretion rates are preferred to maintain higher water storage capacity in the restored tidal marshes. When the objective is to restore intertidal habitats and meet ~~certain~~ specific biodiversity goals (Hinkle and Mitsch, 2005; Chang et al., 2016), it may be favorable for accretion rates to be high so that vegetation can develop fast, but also not too fast so that a diversity of habitats can persist over time, including tidal channels, mud flats, pioneer marsh and higher marsh vegetation, while avoiding a rapid succession to climax species. In the case studied here, our model predicts that the reference restoration design can achieve the objective of intertidal biodiversity rehabilitation. Indeed, because of the relatively slow

accretion rates in the Northern basin (Fig. 6), the restored tidal marsh still features the entire range of intertidal habitats after 50 years (Fig. 3).

l.502: that -> this

Sect. 4.1 (3rd paragraph)

The examples above illustrate the need to identify restoration design options that can steer rates of sediment accretion and vegetation development in line with restoration objectives. In this study, we focus on the impact of one specific design option: the inlet width (Fig. 2). Our model predicts that, for the setting studied here, higher differences between the two inlet widths lead to more contrasting sedimentation and vegetation patterns in the two basins (Fig. 9). This has two positive outcomes. On the one hand, high accretion rates in the Southern basin bring fast vegetation development there, and potentially positive public perception for the restoration project. On the other hand, lower accretion rates in the Northern basin allow for long-term persistence of habitat diversity, which is an important objective in this project. Other important design options, such as the excavation of a channel network (Williams et al., 2002; Wallace et al., 2005; Hood, 2014), the manual planting of vegetation (O'Brien and Zedler, 2006; Staver et al., 2020), the infilling or lowering of areas, or the creation of a landward slope, were beyond the scope of this study. However, new fundamental insight on the impact of such design options is crucial and should be investigated in the future. Our novel biogeomorphic model is made available for the scientific community in ~~that~~ this perspective (see Code and data availability).

Referee #2

The authors present an eco-geomorphological model with many interesting and novel features and apply the model to a design of a restoration project consisting of breaching of an existing dyke. The paper is very valuable as an application of state-of-the-art modelling to a specific restoration site with all the associated complications and uncertainties.

We thank the referee for their careful review of our manuscript, as well as for their positive and constructive remarks.

A critical feature of the model is that it can predict channel formation within the marsh as a result of the new hydrodynamic configuration due to the dyke breaches. It would be very useful to provide more detail on how the process of channel formation is implemented in the model. Is there a threshold value of shear stress? Is that a model parameter that is adjusted or calibrated? How does it compare to other sites/models?

Channels form through erosion and deposition of sediments, following Eq. (S5) to (S7). The critical shear stress for bed erosion is 0.5 N/m^2 for the fresh layer (i.e., sediments deposited during the simulation – Table S3) and 0.8 N/m^2 for the compacted layer (i.e., the sediment bed soil already present before marsh restoration – Table S3). This approach is consistent with a previous study on consolidation of accretional mudflats for the same tidal marsh restoration project (Zhou et al., 2016).

Sect. S1.5.1

The initial bed elevation is based on the project design (Sec. 2.2 and Fig. 2) and Lidar data before de-embankment. The bed is initially exclusively composed of a compacted layer. Tides are imposed into the system by defining water levels and flow velocities at the open boundary between the study site and the Scheldt Estuary, which is here approximately the isobath 5 m below the mean low water level. These boundary conditions are provided by a 3D hydrodynamic model of the estuary, which has been calibrated for a spring-neap cycle by comparison with measurements of water levels, flow velocities and water discharges (Maximova et al., 2014). To reduce the computational time, we do not simulate the entire range of tidal conditions of a full spring-neap cycle. Instead, we only select four different semi-diurnal tidal cycles from the estuarine model, which are representative of the standard range of tidal conditions that can be observed in that area. With high water levels of 2.05, 2.55, 2.87 and 3.25 m NAP, the selected tidal cycles have a frequency distribution of respectively 14.6%, 27.4%, 32.3% and 25.7%, as compared to historical measurements during the period 2007-2017. These frequency distributions are then used to determine the morphological acceleration factor α used for each semi-diurnal tidal cycle (Sec. 2.1). We simulate the impact of sea level rise by lowering the bed elevation every year by a value corresponding to the yearly increase of mean sea level. The suspended sediment concentration at the open boundary is constant and determined based on reported measurements (Vandenbruwaene et al., 2014; Sec. S2). All parameter values used in the hydro-morphodynamic module are based on previous studies in the same restored tidal

marsh area (Maximova et al., 2014; Zhou et al., 2016), the Scheldt Estuary (van Leussen, 1999; Van de Broek et al., 2018) and other intertidal environments (D'Alpaos et al., 2021). They are summarized in Table S3. The suspended sediment concentration at the open boundary and the rate of sea level rise vary according to model scenarios (Table 1).

Deposition of sediment and surface accretion is also quite important for the model results and there are a couple of points that would be good to have more information on. The first one is about the biological component of accretion, which includes the incorporation of plant litter into the soil (Morris et al., 2002) and that is not included in the model. It may well be that is not as important in this setting, but a comment on this would be valuable. For example, Breda et al. (2021) showed that the biological accretion can be of similar magnitude than the sediment related accretion. Those two accretion components may have a different behavior under climate change scenarios.

Sediment accretion in marshes of the Scheldt Estuary is dominated by the external supply by tides of suspended sediments, mostly of mineral nature, while organic matter only accounts for about 10% of the measured accretion rates (Temmerman et al., 2004). For this reason, our model does not explicitly simulate organic matter accretion locally produced by vegetation. However, organic matter accretion can be considered as implicitly compensated for by model calibration for total sediment accretion on vegetated platforms (Sect. 2.4.1). The calibration is indeed based on observed elevation changes, hence total accretion rates, including both mineral and organic contributions.

Sect. 2.2 (2nd paragraph)

Local environmental conditions are determinant for the development of restored ecosystems (Liu et al., 2021). The Scheldt Estuary, here defined as the tidal part of the Scheldt River, is a semidiurnal macrotidal estuary extending over 160 km. At a gauge station near Bath (Fig. 2b), the tidal range has been recorded to vary on average from 4.21 m at neap tides to 5.76 m at spring tides during the period 2011-2015, and the MHWL to rise at a rate of 5.7 mm yr^{-1} during the period 1931-2004 (Wang and Temmerman, 2013). This MHWL rise rate is used here as proxy for SLR rate (Sect. 2.3). The study site lies in the brackish zone of the estuary, which is characterized by a steep gradient in salinity, with values ranging from 5 to 18 PSU (Van Damme et al., 2005; Meire et al., 2005). Therefore, only a limited number of vegetation species (Sect. 2.1) can cope with the local environmental conditions. ~~Finally, the~~ The local SSC is influenced by the presence of a maximum turbidity zone, where large volumes of cohesive sediments are concentrated and continually resuspended by the tidal flow (Baeyens et al., 1997; Chen et al., 2005; Meire et al., 2005). At the study site, the current average SSC is estimated at 63 mg l^{-1} (Sect. S2, supplementary material). Sediment accretion in marshes of the Scheldt Estuary is dominated by the external supply by tides of suspended sediments, mostly of mineral nature, while organic matter only accounts for about 10% of the measured accretion rates (Temmerman et al., 2004). For this reason, our model does not explicitly simulate organic matter accretion locally produced by vegetation.

The other point is the formulation for deposition of fine sediment. Cohesive sediment deposition often involves the determination of a minimum depositional velocity below which fine particles (colloids) remain in suspension (Metha and McAnally, 2008). The model used in the paper does not have a minimum velocity threshold in its formulation, so it would be good to discuss the implications of such approach.

The existence of a minimum depositional velocity (or shear stress) below which fine particles remain in suspension is debated in the literature. In our model, we follow one of the well-established arguments that such threshold does not exist, and that it rather represents a threshold for erosion of freshly deposited sediments (Winterwerp, 2007). This approach agrees with field observations in the Chesapeake Bay (Sanford and Halka, 1993) and is often adopted in recent biogeomorphic models (e.g., Adams et al., 2016; Bryan et al., 2017; Mariotti, 2018; Zhang et al., 2019; Brückner et al., 2020).

Sect. S1.1 (3rd paragraph)

Sisyphe solves the depth-averaged advection-diffusion equation to simulate fluctuations of the depth-averaged suspended sediment concentration C:

Equation (S4)

where E and D are the rates of sediment erosion and deposition, respectively. The rate of sediment erosion is computed using the equation of Partheniades (1965):

Equation (S5)

where M is the Partheniades constant and τ_e is the critical bed shear stress for sediment erosion. The rate of sediment deposition is computed using the equation of Einstein and Krone (1962):

Equation (S6)

where w_s is the sediment settling velocity. The existence of a threshold shear stress below which sediments remain in suspension is debated in the literature. Here we follow one of the well-established arguments that such threshold does not exist, and that it rather represents a threshold for erosion of freshly deposited sediments (Winterwerp, 2007). This approach agrees with field observations in the Chesapeake Bay (Sanford and Halka, 1993) and is often adopted in recent biogeomorphic models (e.g., Adams et al., 2016; Bryan et al., 2017; Mariotti, 2018; Zhang et al., 2019; Brückner et al., 2020).

References

Only references cited in referee's comments and author's responses are reproduced here.

Bayliss-Smith, T.P., Healey, R., Lailey, R., Spencer, T., and Stoddart, D.R.: Tidal flows in salt marsh creeks, Estuar. Coast. Shelf S., 9, 235-255, https://doi.org/10.1016/0302-3524(79)90038-0, 1979.

Breda, A., Saco, P.M., Sandi, S.G., Saintilan, N., Riccardi, G., and Rodríguez, J.F.: Accretion, retreat and transgression of coastal wetlands experiencing sea-level rise, Hydrol. Earth Syst. Sc., 25, 769-786, https://doi.org/10.5194/hess-25-769-2021, 2021.

French, J.R. and Stoddart, D.R.: Hydrodynamics of salt marsh creek systems: Implications for marsh morphological development and material exchange, Earth Surf. Proc. Land., 17, 235-252, https://doi.org/10.1002/esp.3290170304, 1992.

IPCC: IPCC Special Report on the Ocean and Cryosphere in a Changing Climate, 2019.

Mehta, A.J., and McAnally, W.H.: Fine-grained sediment transport, in: Sedimentation engineering: processes, management, modeling and practice, edited by: Garcia, M.H., American Society of Civil Engineers, Reston, VA, USA, 2008.

Morris, J.T., Sundareshwar, P.V., Nietch, C.T., Kjerfve, B., and Cahoon, D.R.: Responses of coastal wetlands to rising sea level, Ecology, 83, 2869-2877, https://doi.org/10.2307/3072022, 2002.

Pethick, J.S.: Velocity surges and asymmetry in tidal channels, Estuar. Coast. Shelf S., 11, 331-345, https://doi.org/10.1016/S0302-3524(80)80087-9, 1980.

Schwarz, C., Gourgue, O., van Belzen, J., Zhu, Z., Bouma, T.J., van de Koppel, J., Ruessink, G., Claude, N., and Temmerman, S.: Self-organization of a biogeomorphic landscape controlled by plant life-history traits, Nat. Geosci., 11, 672-677, https://doi.org/10.1038/s41561-018-0180-y, 2018.

Silinski, A., van Belzen, J., Fransen, E., Bouma, T.J., Troch, P., Meire, P., Temmerman, S.: Quantifying critical conditions for seaward expansion of tidal marshes: A transplantation experiment, Estuar. Coast. Shelf S., 169, 227-237, https://doi.org/10.1016/j.ecss.2015.12.012, 2016.

Temmerman, S., Govers, G., Wartel, S., and Meire, P.: Modelling estuarine variations in tidal marsh sedimentation: response to changing sea level and suspended sediment concentrations, Mar. Geol., 212, 1-19, https://doi.org/10.1016/j.margeo.2004.10.021, 2004.

Vandenbruwaene, W., Bouma, T.J., Meire, P., and Temmerman, S.: Bio-geomorphic effects on tidal channel evolution: impact of vegetation establishment and tidal prism change, Earth Surf. Proc. Land., 38, 122-132, https://doi.org/10.1002/esp.3265, 2013.

Vandenbruwaene, W., Schwarz, C., Bouma, T.J., Meire, P., and Temmerman, S.: Landscape-scale flow patterns over a vegetated tidal marsh and an unvegetated tidal flat: Implications for the landform properties of the intertidal floodplain, Geomorphology, 231, 40-52, https://doi.org/10.1016/j.geomorph.2014.11.020, 2015.

Zhou, Z., van der Wegen, M., Jagers, B., and Coco, G.: Modelling the role of self-weight consolidation on the morphodynamics of accretional mudflats, Environ. Modell. Softw., 76, 167-181. https://doi.org/10.1016/j.envsoft.2015.11.002, 2016.